Journal of Intelligent and Robotic Systems **27:** 171–193, 2000.

The Formula One Tire Changing Robot (F1-T.C.R.)

RAUL MIHALI and TAREK SOBH
Department of Computer Science and Engineering, University of Bridgeport, Bridgeport, CT 06601, USA; e-mail: sobh@bridgeport.edu

(Received: 16 June 1998; in final form: 6 April 1999)

Abstract. Formula One racing is one of the most fascinating sports ever, it is a perfect combination of high speed, technology, pressure and danger. One problem associated with car racing is the time differential between teams during pits stops, which substantially affects the final results. In addition, a high percentage of the accidents in Formula One is due to pit stop problems. Changing the tires of a car while almost in motion, after reaching dangerous pressure and temperature values, is a very risky challenge, no matter how well a team is trained. Approximately 15–25 people are constantly exposed to serious dangers. The risks taken are extreme and any idea of reducing it without affecting the quality of the race should be considered. Our idea is to build a fully robotized system that takes over the tire changing and refueling process. There will practically be no need for human intervention. The system will demonstrate remarkable time accuracy, precision and low risk implications, uniformity of performance across teams, the competition being relayed solely upon the pilots.

Key words: robotics, car racing, robotic application, tire changing, Formula One.

1. Introduction

A high percentage of Formula One racing accidents occurs due to pit stop problems. Changing the tires of a car while almost in motion, after moving at speeds of 300 km/h and reaching dangerous pressure and temperature values, is a very risky challenge for human beings, no matter how well trained they are.

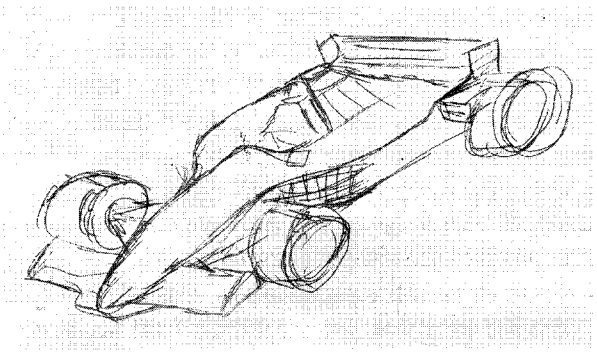

Figure 1. Car model.

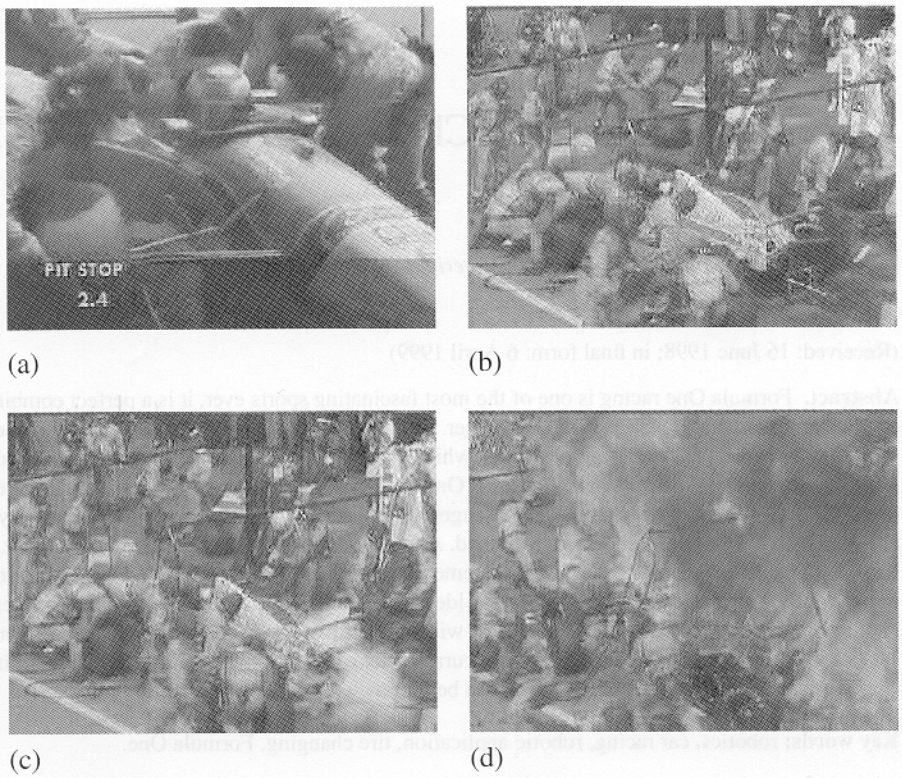

Figure 2. (a) Pit stop accident (I); (b) Pit stop accident (II); (c) Pit stop accident (III); (d) Pit stop accident (IV).

In the following example, due to the malfunctioning of the refueling-equipment, the entire team including the pilot had to risk their lives; accident off the Benneton team, Joe Verstappen's car, 1994, Germany.

A second problem of the pit stop is the considerable time difference between teams in the tire changing process. Suppose the team of the pilot currently on the second position can change the tires of their car in 8 s, while the team of the pilot from the pole position can do it only in 16 s. They usually do much better than that, however, today they seem not to coordinate that well. Such a difference will most probably change the position of the two pilots at the end of the race. While many fans consider it an exciting part of the race, it is not competitive at all because there is a great chance of not being able to keep such a time constant while working with 15–20 people. Even though this second problem of pit stops is a matter of taste, the high human risk implication still remains a key reason for a robotized solution. Watching a race with the idea that you might see fatal accidents while you clearly know that they can be avoided is unacceptable. The system presented here eliminates the presence of any team member around a car while in pits stop,

assures an excellent quality of pit servicing and maintains the pit stop time constant, thus minimizing the risks on the pilot and improving the quality of the race.

1.1. PROBLEMS ENCOUNTERED/PERFORMANCE

In order to maintain the pit time low and constant, the first parameter to be optimized should be the *time accuracy*. More specifically, the robot has to change the tires of any car within the same time quantum. The current variance of *seconds* achieved by pit stop teams requires remarkable experience, but does not prove sufficient in a race, almost always affecting the final position of the pilots. A precision of 0.1 s or better between any two teams is required.

In the first version of our proposed system, a process length of 15–18 s will be achieved, and will be optimized to 6–8 s later.

Usually a pilot cannot stop easily in the pits with a precision of less than 5 cm or so. However, the manipulator needs it while working with the tires. Therefore, a sensor system will be implemented.

Another constraint is the *environment's limitations*. Only moderate changes in the pit stop's configuration can be allowed, due to the severe FIA regulations.

2. Brief Mechanical Approach

2.1. PRAGMATIC CONSIDERATIONS/ARMS REQUIRED/WORKSPACE

Our proposed robotic system consists of 5 manipulators: one for each of the tires, and a fifth one for the fuel tank. To preserve the environment of the pit stop and to assure the comfort of the team we implement suspended manipulators. The support of the five arms (Figure 3) allows the sliding motion of each arm and also does not create any obstacles or driving difficulties for the pilot.

The support has two double longitudinal branches on which the arms will be suspended, two arms on one pair of branches (sliding zone B), and three on the

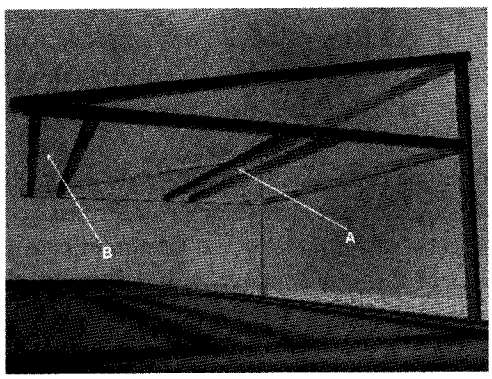

Figure 3. View from the track side.

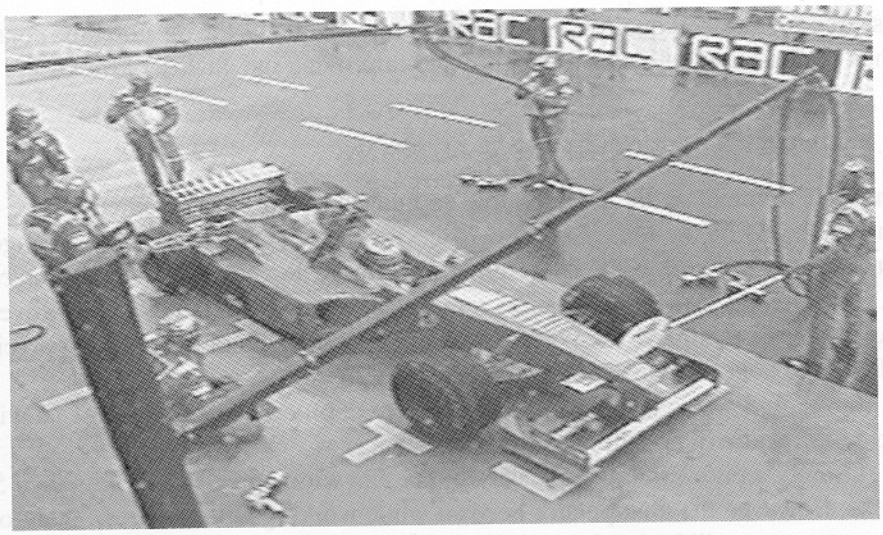

Figure 4. Typical Formula One car.

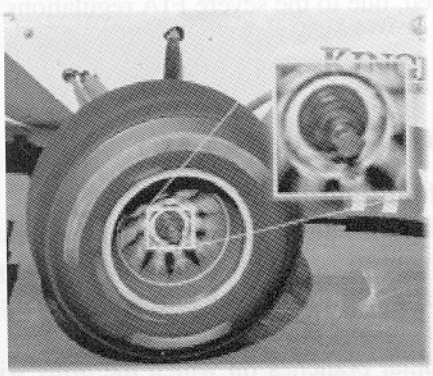

Figure 5. Tire close-up.

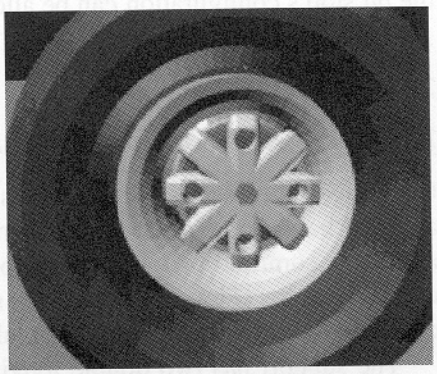

Figure 6. Tire CAD design.

other one (sliding zone A). The sliding mechanism of the arms proves to be essential for the end-effector positioning. The material has to be resistant, of low elasticity and capable of sustaining the mass of the arms. An extremely resistant and rigid material needs to be used.

Because a wheel of a Formula One car is attached with a single central screw (see Figure 5), there is design space for a flexible end-effector, with less required torque and mass. The multi-screw wheels from streetcars would complicate significantly the system, a different version of this robot is currently being considered for that purpose too.

Figure 5 shows a close-up of the "one screw" tire and Figure 6 shows a CAD design of a tire as it will be displayed after the sensor system interprets the position of the four wheel holes.

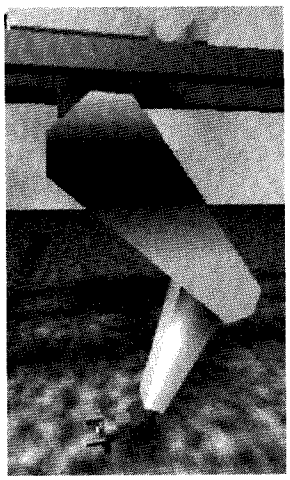

Figure 7. Side view.

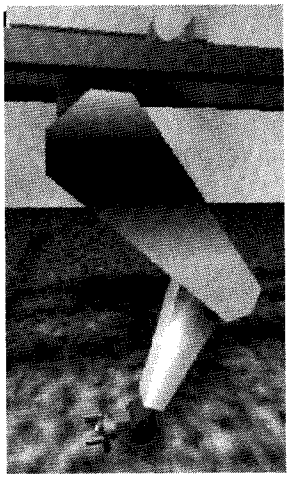

Figure 8. Front view.

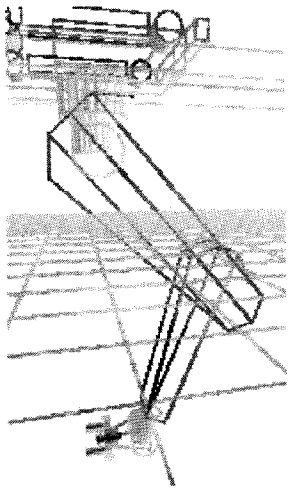

Figure 9. Wire-frame side view.

Each of the manipulators has a sliding range of (1–1.5 m on the supports and can handle a tire in many ways. The only plane in which a good dexterity is required is the horizontal one, due to the fact that the distance from the ground and the tire's central axis is relatively constant (a certain tolerance will be assumed). Based on the above-mentioned requirements, the manipulator design in Figures 7–9 has been reached.

2.2. TASKS AND MOTION RELATED BRIEFINGS

The car arrives into the pits from a certain direction and stops in approximately the same position every time. By the time the car arrives, the robot's sensor system registers it and notes the exact position and direction of the tires. Once the car stops, the arms start the *tire changing process*. For lifting the car, a simple lifting system will be implemented and positioned on the stopping platform, which would suspend the car throughout the whole process. Each tire handling manipulator has to go through the following task sequence:

- Position the end-effector as a function of the tire parameters received from the sensor system.
- Rotate the end-effector so that it can catch the tire.
- Grab the tire.
- Remove the screw.
- Remove the tire from its axis and put it on the ground near the car in a convenient spot.

- Change the position and grab the new tire, located in the proximity, with a new screw on it.
- Position again the end-effector and fix the new tire on the axis.
- Tighten the screw.
- Move back in the *stand-by* position to enable the car's departure.

There are about 15 different moves to be done, each one in about 1 s, which would allow a process length of approximately 15 s per manipulator. Of course, all the arms work in parallel and independently.

The positioning of the end-effector and actually the entire set of movements required are of short distance and mainly consist of revolute steps: arm expansion/contraction, arm/end-effector rotation and end-effector positioning. There is a good probability that the specified time of one second per move can be reduced.

Four microsensors will be mounted on each tire, responsible for specifying the tire's angle and position relative to the arm. According to the information from these sensors, the end effector can position itself perpendicularly on the tire and grab it correctly. We did not have yet the chance to work on a racecar, but the system can be easily adjusted in case the dimensions vary a bit from the one we considered.

The rotation of the screw is a simple task, implying the activation of one compressed air tool located in the end-effector.

The most time-consuming task is handling of the tire itself. This task requires good torque and acceleration control on the entire arm, implying the activation of all the engines, including precision sliding. The time interval from removing the old tire and replacing it with the new one it is estimated to be approximately 3–5 s. A team member will position the replacement tires in the proximity of each arm before the car would arrive in the pits

Moving back in the stand-by position is again a simple task and can be completed partially when the car leaves. As long as the arms are at a safe distance from the tires the car can be ready to go.

Because of the sliding mechanism, the pilot can allow errors of up to half a meter while parking. However, there are still some exceptional positions, which will require special attention.

2.3. JOINT/LINK REQUIREMENTS AND CONSTRUCTION

One arm is composed of 4 joints and the end-effector. The first joint is a prismatic one, constituted by the sliding part of the system, as shown in Figures 10 and 11. Figures 10 and 11 depict a sketch of the actual mechanism, a view from the top of the robot with the car behind on the left and on a general view from beneath the arm on the right taken from the car's side, driver's position. The prismatic movement is controlled by one motor fixed as shown. The torque/mass ratio of the motor does not have to be stringent, and a sliding accuracy of 1 mm should

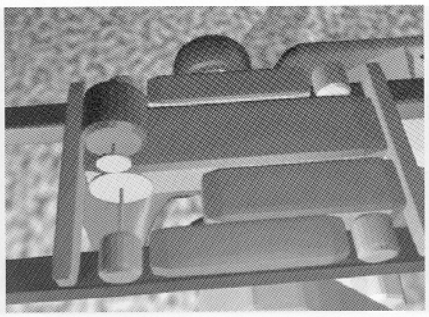

Figure 10. The slider (top).

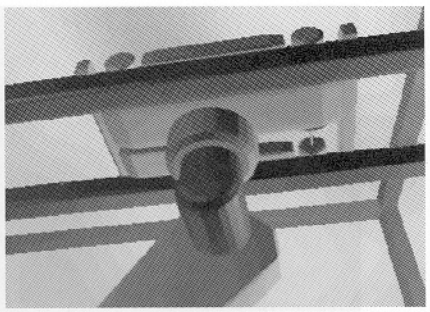

Figure 11. The slider (beneath).

Figure 12. Second joint view I.

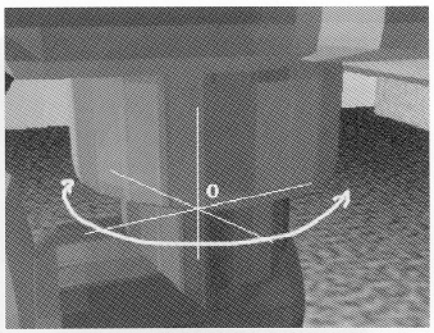

Figure 13. Second joint view II.

be sufficient. Typically, the slider is activated just in the beginning of the full tire changing process, in order to fix the arm in an appropriate position. The friction coefficient of sliding between the support and the four wheels has to allow a stable braking with a precision of 1 m/s^2 and the friction coefficient of revolution has to allow low acceleration control.

The joint has a braking mechanism (not visible in the figure) which activates once the requested position has been achieved. This will simply lock the arm on the support while changing the tire, thus reducing the resultant of the vertical and horizontal vibrations. All arm motors work at high speed, have significant mass, and so the inertia problem has to be considered carefully [5, 7, 11].

Controlling this joint is the easiest task as long as it does not have to be part of the robot's equations. To use time optimally, the arm will move – from/to – the stand-by position – to/from – the ready position in the same time with the sliding action (more details in the *Controlling* and *Parameters* related sections).

The second joint is a revolute one, as are all of the following ones. The next four Figures (12–15) show the joint and indicate the rotation direction. The view is from the bottom left of the joint (car side) in Figures 12–14 and the view is from above, right side in Figures 13–15 – Phong and wireframe views.

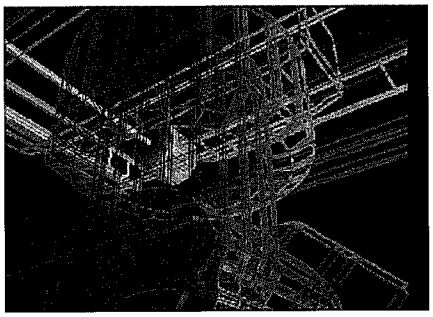

Figure 14. Second joint view I (wire-frame).

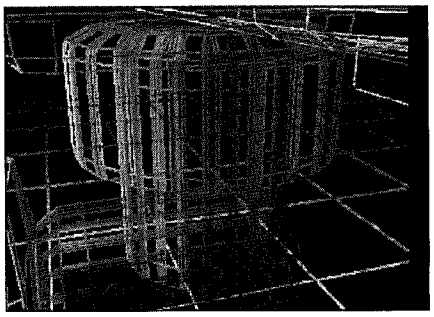

Figure 15. Second joint view II (wire-frame).

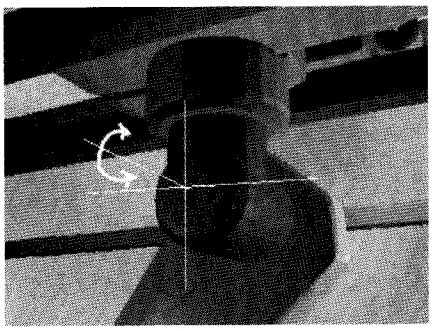

Figure 16. Third joint view I.

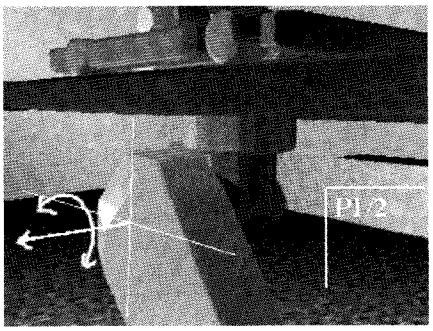

Figure 17. Third joint view II.

The second joint is an essential orientation joint and is controlled by a strong motor, because it supports most of the tensions of the other motors and masses. A revolution limitation of (3/2) PI might seem subjective, but limiting it does not create kinetic or dynamic problems (e.g., singularities). The motor is fixed in the sliding part, thus allowing flexibility in mass, the pressure now being moved on the normals between the support and the 4 wheels of each slider.

The third joint is closely mounted near the previous one, and together with it and the sliding joint forms the *static* main concentration of mass and torque of the arm. Figures 16, 18 show the view from the car's side, under the slider and Figures 17, 19 show the view from the arm side on the right.

It is necessary to keep a high torque in this part of the arm, to allow a better torque control for the next joints while a tire is being manipulated. Thus, the motor of this joint has to be attached to the axis of the previous joint, which will remain locked while manipulating the tire. The remainder of the arm has to be as light as possible because it forms the *transportable* part of it (due to the fact that it will be the only one moving once the static part finishes its task). The angle of rotation has been limited to less than PI/2 degrees (singularity reasons).

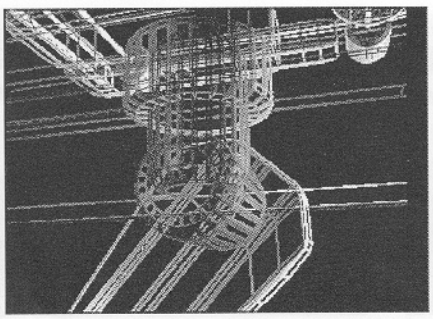

Figure 18. Third joint view I (wire-frame).

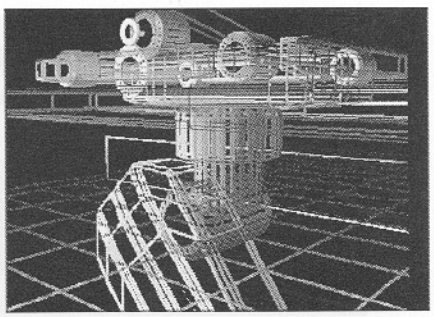

Figure 19. Third joint view II (wire-frame).

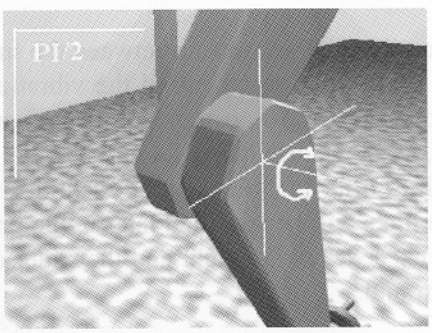

Figure 20. Elbow joint view I.

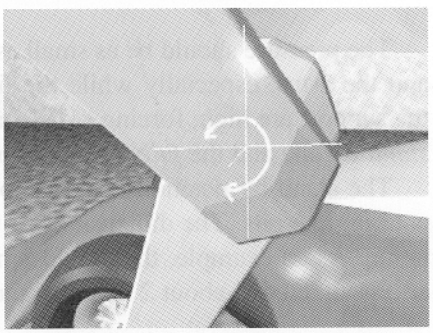

Figure 21. Elbow joint view II.

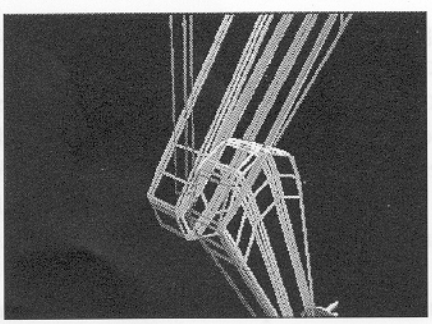

Figure 22. Elbow joint view I (wire-frame).

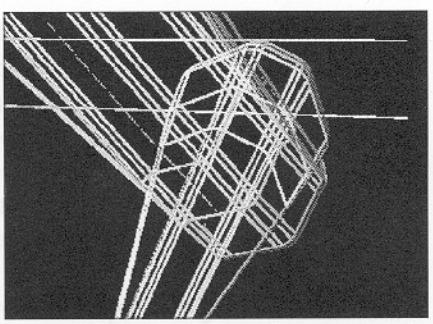

Figure 23. Elbow joint view II (wire-frame).

The last revolute joint from the arm segment is the elbow joint (shown in Figures 20–23). This joint's motor should be light and has a relatively small torque. The transportable part of the arm has to be as light as possible in order to achieving the required speed and torque. It is installed in the upper part of the arm, thus keeping a safe distribution of mass. The angle of revolution has been limited to no more than PI/2 degree again. This range fits the requested tasks and also does not create singularities.

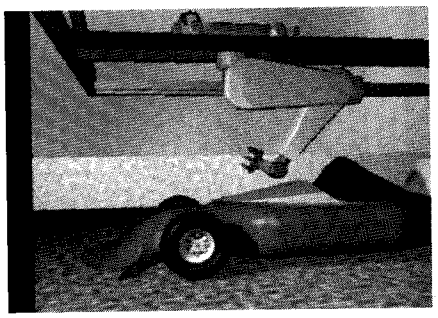

Figure 24. Stand-by position.

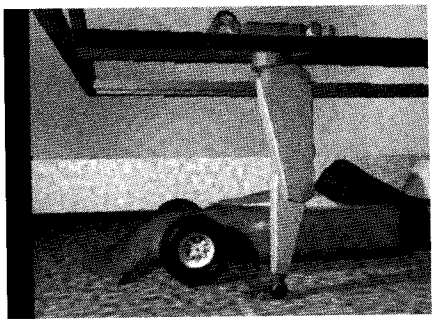

Figure 25. Fully extended position.

The pressure should be as small as possible on the contacts between the support and the arms, especially while the five arms work together and the vibrations in the support are high, forcing a dislocation. The critical positions of the arm are the *stand-by* one and the *fully extended* one, as shown in Figures 24 and 25.

The stand-by position is safe enough to offer the pilot a good visibility while entering the pits. The dimensions of the links will be specified later in the presentation. As an example, the car does not exceed 1 m in height and the slider of the arm is situated at about 2 m above the ground.

2.4. THE END EFFECTOR (DESIGN/JOINTS/DEXTERITY/POWER/ACCURACY)

The end-effector has to be small and light, but powerful, dexterous and quick. In the early stages of the design, we opted for a double-ended effector design. This would have allowed a faster manipulation of the tires because it would not require the arm to put the tire down and grab the new one. The arm would get loaded with the new tire at one of the sides of the effector, the one opposite to the car. When the car would stop, the other side of the effector would remove the screw and grab the used tire, then do a PI degree rotation on the central vertical axis and attach the new tire to the car body.

After calculating the required dimensions and torque for the materials and engines, the results were discouraging, the required torque being not realistic. Another problem that became apparent was the high vibration in the entire system. Once the end-effector would spin, a helicoidal path of motion would get employed, resulting in strong moments tending to dislocate the arm from the support, pulling it up.

After trying few more designs, we stopped at the one from Figure 26. This is a single ended-effector, a change that was necessary, to avoid the high forces from the supports.

This model solved all the problems so far. First, there are no more positioning problems. The disk type effector can rotate at a speed ω_2, and reach any orientation requested by the sensor system. Having four identical tools, there would not be any

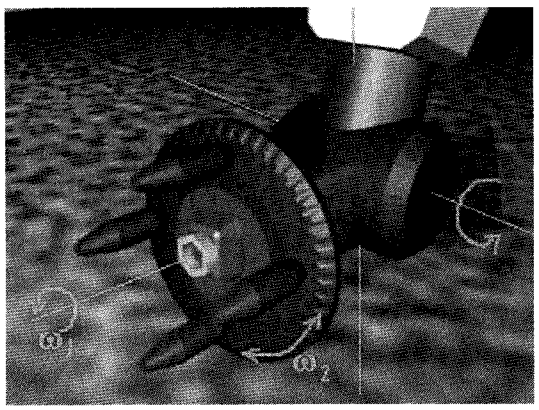

Figure 26. End-effector (final design).

more equilibrium problems during transportation. The electro-magnetic forces are well distributed now and allow movements within a wide acceleration range.

The revolute joint between the arm and the effector allows a rotation in the vertical plane of PI/2 degrees. The motor is installed in the cylinder in order to allow for uniform mass distribution in the entire arm. The motor that spins the disk with the four side segments is installed in the pyramidal body following the cylinder. In the same spot the compressed-air system is installed (for screw-removal).

The only rotation that cannot be performed by this end effector is the one on the vertical axis. This one, however, it is covered by the first revolute joint at the base of the arm, which supports most of the torque and allows for good acceleration control. So at this point the end effector is able to operate for almost any reachable position of the tire. Another advantage of this arm style is that the tire does not have to be perpendicular to the ground (supposing an accident has happened). The end effector would still be able to accommodate the correct orientation. However, once the tire is not perpendicular to the ground this would mean that the car has been damaged seriously and most probably needs intervention of the team (another advantage of mounting sensor in the tires).

Another issue to be clarified is the way in which the compressed air screwdriver finds the position of the screws: The screw driver starts a revolute task and at the same time tries to advance slowly until it "fits" the faces of the screw and fixes onto the screw.

The arm without the end-effector, the sliding mechanism and its very rigid structure requirements, it is kinematically very similar to the PUMA 560 arm series ([9, 12, 19]) and we are considering to refurbish a PUMA arm for testing purpose.

3. Direct and Inverse Kinematics Approach

One of the next steps is solving the direct and inverse kinematics for this specific manipulator (Figure 27).

Here, 6 joints of the arm can be seen. Using the Denavit–Hartemberg table [2], the equations for the direct kinematics can be written as (the dimensions of the links are known):

$$
\begin{aligned}
x &= L + \cos(\theta_1) \cdot (\mathrm{S2}\sin(\theta_2) - \mathrm{S3}\sin(\theta_2 + \theta_3) - \mathrm{S4}\sin(\theta_2 + \theta_3 + \theta_4 - \mathrm{PI}),\\
y &= -\sin(\theta_1) \cdot (\mathrm{S2}\sin(\theta_2) - \mathrm{S3}\sin(\theta_2 + \theta_3) - \mathrm{S4}\sin(\theta_2 + \theta_3 + \theta_4 - \mathrm{PI}),\\
z &= \mathrm{S1} + \mathrm{S2}\cos(\theta_2) - \mathrm{S3}\cos(\theta_2 + \theta_3) - \mathrm{S4}\cos(\theta_2 + \theta_3 + \theta_4 - \mathrm{PI}),\\
\theta_x &= 0,\\
\theta_y &= 3\mathrm{PI}/2 - (\theta_2 + \theta_3 + \theta_4),\\
\theta_z &= \theta_1,
\end{aligned}
$$

where x, y, z, are the coordinates and θ_x, θ_y, θ_z the orientations of the end-effector.

Solving for the inverse kinematics using direct algebraic methods [18], we obtain the following model (note that we are using kinematic decoupling, only solving for a 3×3 matrix, then again for a 3×3 one for the end effector).

$$
\begin{aligned}
L &= \big(y/\tan(\theta_z)\big), \qquad \theta_1 = \theta_z,\\
\theta_3 &= \arccos\Big(\big(\mathrm{S2}\cdot\mathrm{S2} + \mathrm{S3}\cdot\mathrm{S3} - \big(x + \mathrm{S4}\sin(\mathrm{PI}/2 - \theta_y)\cdot\cos(\theta_z) -\\
&\quad -\big(y/\tan(\theta_z)\big)\big)\cdot\big(x + \mathrm{S4}\sin(\mathrm{PI}/2 - \theta_y)\cdot\cos(\theta_z) - \big(y/\tan(\theta_z)\big)\big) -\\
&\quad -\big(z + \mathrm{S4}\cos(\mathrm{PI}/2 - \theta_y) - \mathrm{S1}\big)\times\\
&\quad \times\big(z + \mathrm{S4}\cos(\mathrm{PI}/2 - \theta_y) - \mathrm{S1}\big)\big)/(2\mathrm{S}\cdot 2\mathrm{S3})\Big),\\
\theta_2 &= \arccos\Big(\big(-\big(\mathrm{S3}\sin(\theta_3)\big)\big(\big(x - \big(y/\tan(\theta_z)\big)\big)/\cos(\theta_1) + \mathrm{S4}\sin(\mathrm{PI}/2 - \theta_y)\big) +\\
&\quad + \big(\mathrm{S2} - \mathrm{S3}\cos(\theta_3)\big)\cdot\mathrm{sqr}\big(\big(\mathrm{S2} - \mathrm{S3}\cos(\theta_3)\big)\big(\mathrm{S2} - \mathrm{S3}\cos(\theta_3)\big) +\\
&\quad + \big(\mathrm{S3}\sin(\theta_3)\big)\big(\mathrm{S3}\sin(\theta_3)\big) - \big(\big(x - (y/\tan(\theta_z))\big)\big)/\cos(\theta_1) +\\
&\quad + \mathrm{S4}\sin(\mathrm{PI}/2 - \theta_y)\big)\big(\big(x - (y/\tan(\theta_z))\big)\big)/\cos(\theta_1) +\\
&\quad + \mathrm{S4}\sin(\mathrm{PI}/2 - \theta_y)\big)\big)\big)/\big(\big(\mathrm{S2} - \mathrm{S3}\cos(\theta_3)\big)\cdot\big(\mathrm{S2} - \mathrm{S3}\cos(\theta_3)\big) +\\
&\quad + \big(\mathrm{S3}\sin(\theta_3)\big)\big(\mathrm{S3}\sin(\theta_3)\big)\big)\big)\Big),\\
\theta_4 &= 3\cdot\mathrm{PI}/2 - \theta_y - \theta_2 - \theta_3.
\end{aligned}
$$

Figure 28 proves to be helpful when describing the position and orientation of the end-effector in terms of the tire's coordinates, obtained from the sensor system.

The metrics referred to are as shown in Figure 29:

α = The angle between the tire and the normal to the slider.

P = The position of the end-effector.

H = The distance between the slider and the car.

I = The distance from the center of the tire to the center of the slider.

λ = The distance from the center of the tire to the position of the end-effector.

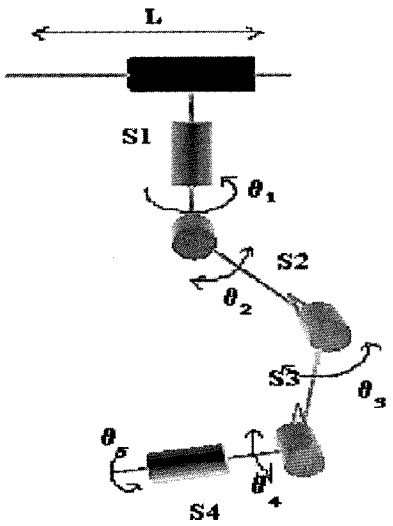

Figure 27. Manipulator scheme A.

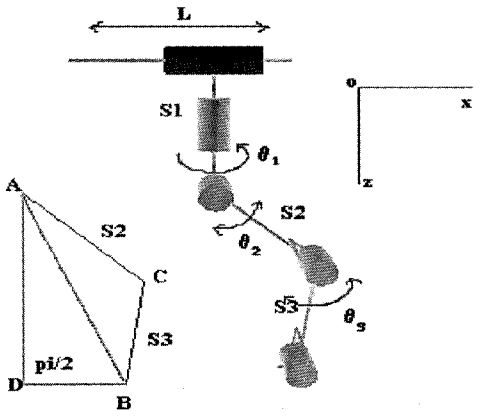

Figure 28. Manipulator scheme B.

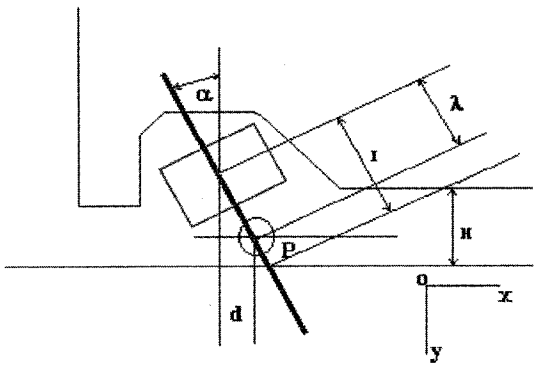

Figure 29. Front left tire scheme (top).

The origin of $xyzO$ is situated at the left end of the slider and so we have a positive moving distance. The positions of the tire are referred by the sensor system to the same $xyzO$. Specific dimensions for the lengths and other metrics are available in the software package.

For the first joint the angle does not have to exceed PI degrees (see Figure 31). As initial position (or stand-by), the angle will be always positioned at 0 degrees. The following 3 joints have been referred in terms of the previous link direction.

For joint 2 (Figure 32) the angle does not have to exceed PI/2. The angle will reach a value close to 0 degree very rarely (when the car is situated further away from the arm, about 80 cm or more). The initial position of this angle will be set close to PI/2, so the link will go up.

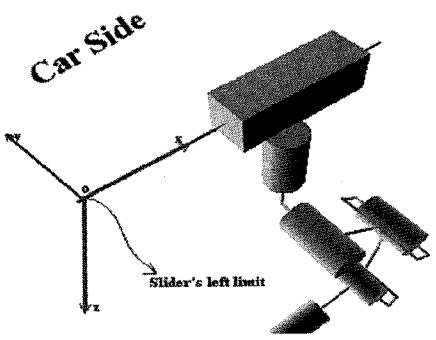

Figure 30. The slider.

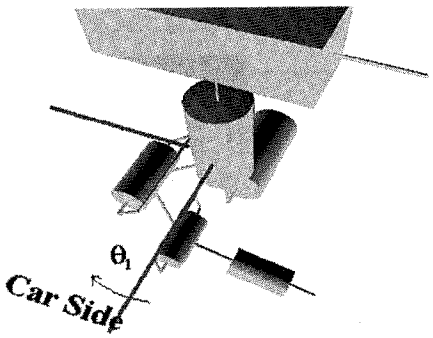

Figure 31. Second joint.

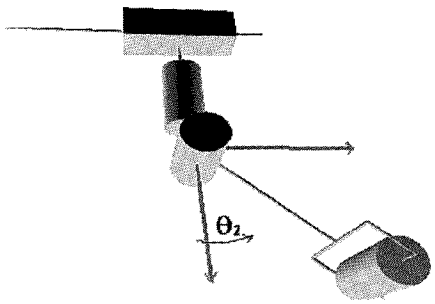

Figure 32. Third joint.

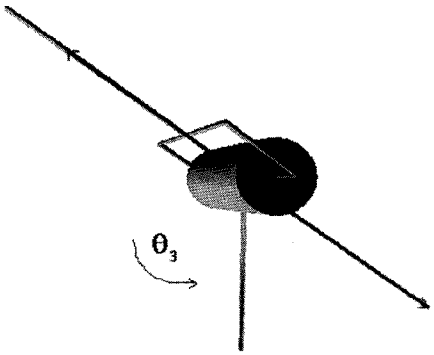

Figure 33. Elbow joint.

For joint 3 (Figure 33), the reference to the previous link proves a superfluous allowance for the angle, because the architecture of the robot does not allow angles less than PI/12. So we use values between PI/12 and up to PI. For the stand-by position the angle will be set around PI/12.

Joint 4 (Figure 34) has lower limits than physically possible. The angle value should not be smaller than PI/4 and also no bigger than $5 \cdot$ PI/4. Very small angles simply cannot be reached – because of the architecture of the arm. Slightly larger angles (close to PI/4 or $5 \cdot$ PI/4) would cause problems holding the tire. A value of PI/2 is used for the stand-by position and also for the P position – Figure 29.

The final joint (Figure 35) is adjusted independently from the others. The rotation direction matters as regards to controlling the torque. The value can run from 0 up to 2 PI. A software tracking system is being built, allowing rotating the 4 segments synchronously from the moment the sensor system gives information about the tire's position. Thus, the angle can go up to n PI. This might be useful when the achieved speed is not satisfactory and there is a need to position the tools in advance.

For velocity and acceleration kinematics, the equations obtained from the D–H table define a function between the Cartesian space of positions and directions

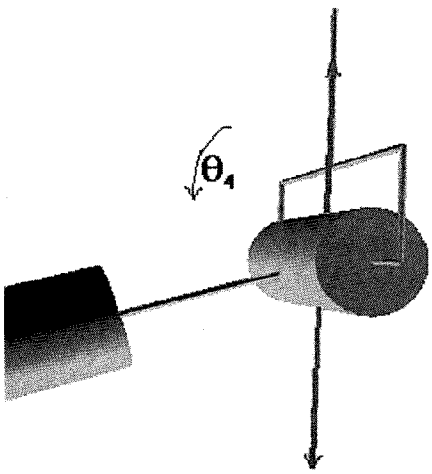

Figure 34. Fourth joint.

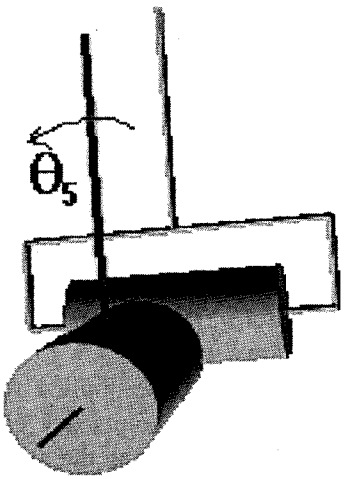

Figure 35. Fifth joint.

and the joint positions. We determine the velocity derivating the Jacobean of this function. Decoupling of singularities is not necessary as long as the design allows the avoidance of these.

The inverse velocity and acceleration are obtained from the following derivations:

$$\dot{\mathbf{q}} = \mathbf{J}(\mathbf{q})^{-1}\dot{\mathbf{x}}, \qquad \ddot{\mathbf{q}} = \mathbf{J}(\mathbf{q})^{-1}\mathbf{b},$$

where

$$\mathbf{b} = \ddot{\mathbf{x}} - \frac{\mathrm{d}}{\mathrm{d}t}\mathbf{J}(\mathbf{q}) \cdot \dot{\mathbf{q}}, \qquad \ddot{\mathbf{x}} = \mathbf{J}(\mathbf{q})\ddot{\mathbf{q}} + \frac{\mathrm{d}}{\mathrm{d}t}\mathbf{J}(\mathbf{q}) \cdot \dot{\mathbf{q}},$$

where

$\mathbf{q}$ = the vector of joint coordinates,
$\mathbf{J}(\mathbf{q})$, $\mathbf{J}(\mathbf{q})^{-1}$ = the Jacobian and inverse Jacobian of $\mathbf{q}$,
$\mathbf{x}$ = the vector of end-effector coordinates.

4. Direct and Inverse Dynamics Approach

For this type of arm the following dynamics model ([1, 2, 4–6]) is used:

$$\begin{aligned} \tau &= \mathbf{M}(\mathbf{q})\ddot{\mathbf{q}} + \mathbf{V}(\mathbf{q}, \dot{\mathbf{q}}) + \mathbf{G}(\mathbf{q}) + \mathbf{F}(\mathbf{q}, \dot{\mathbf{q}}), \\ \ddot{\mathbf{q}} &= \mathbf{M}^{-1}(\mathbf{q})\big[\tau - \mathbf{V}(\mathbf{q}, \dot{\mathbf{q}}) - \mathbf{G}(\mathbf{q}) - \mathbf{F}(\mathbf{q}, \dot{\mathbf{q}})\big], \end{aligned}$$

where:

τ = the end-effector torque, $\mathbf{M}$ = the symmetric joint-space inertia matrix,
$\mathbf{V}$ = describes *Coriolis* and *centripetal* effects [2, 6, 7],
$\mathbf{G}$ = the gravity loading, $\mathbf{F}$ = the end-effector force.

5. The Sensor System. Implementation and Sensing

The variable elements derived from the sensor system that participated in computing the inverse kinematics equations, were Cx, Cy and the angle α made by the tire's axis with the slider (as shown in Figures 36–38). These parameters are required for each tire, so there is a need for four sensor sensing systems. Furthermore, we also need the xyz coordinates of each of the four tire holes. Once we acquire the coordinates of the four holes of one tire, the other variables can be easily deducted, as long as Cx and Cy represent the center of the parallelepiped made by the holes' position and then translated with a constant k representing the width of the tire.

The data that has to be supplied by the sensor system consists of the 3-dimensional coordinates of 16 points (for each tire there are four holes that need to be located). The angle between the axis of the front and rear tires is α. The rear tires will never change the angle relative to the rest of the car. The front tires are parallel, otherwise the car would have serious damages. The tires are always referable to each other, as long as the distance between them is constant (having a variable distance between the tires would result in abnormal situations).

Once we obtain the positions of one of the front tire's holes and one of the rear tires' holes, we can build easily the other coordinates required. Figure 38 depicts the variable angle between the axis of the front and rear tires.

5.1. MOTION ACCURACY

There is a need to control the number of times per second the sensor system provides data ([18, 19]). This is important to determine the car's motion. Motion recovery would allow one arm to track the tire and to have the end-effector positioned even before the car would stop, thus gaining some time. In case the software kinematics solution is slow in real time, a hardware implementation has to be taken in consideration.

5.2. TECHNOLOGICAL ORIENTATION

According to the required sensor system tasks, one of possible implementations for this sensory system can be through a radio radar detector ([13, 14, 17]).

Using video cam systems would complicate the problem because of the high-detail image processing that would be required. There are already built sensor system with accuracy close to our needs, but they prove to be too expensive and resource consuming [15 – 17]. We could also choose a laser scanning system and further complicate the interpretation of the data. So long as four micro-sensors can be installed on the tires, the problem becomes more manageable.

The scanning part of the system situated somewhere close to the scene, would always stay in a scan mode and pick signals from the tires.

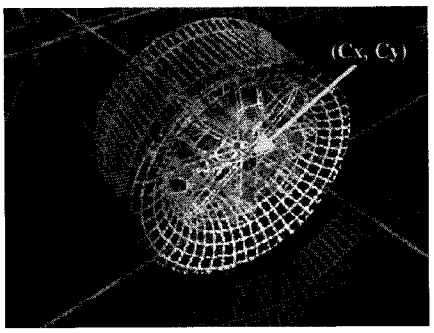

Figure 36. Front left tire (wire-frame close-up).

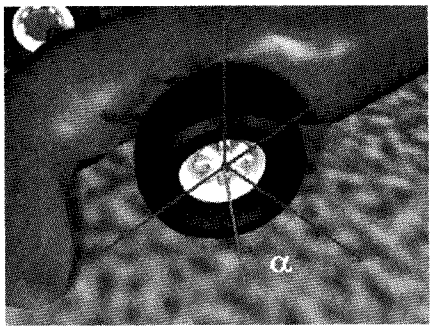

Figure 37. Front left tire (shaded view).

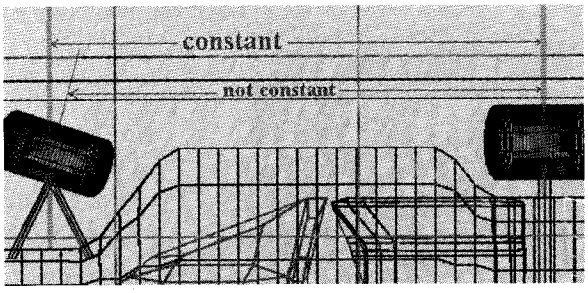

Figure 38. The car (view from above – wire-frame).

The sensors of the tires will be scanned send every tenth of a second. Once the scanner reads the sensors, this implies that the car is situated somewhere close to the pits and according to the distance and the speed of the car the software will process and send the necessary information to the arm controller. Note that the weather condition or other external factors are of minimal effect on this sensing system.

The scanner could get data from the tires each time the car passes near the pits. The skew of the tires can be calculated simply from one frame and represents an extension in 3D of the angle α. For the oscillations we need more frames so that the distance between the ground and tire can be analyzed. This vertical distance Δy can be calculated from two frames having holes at about the same orientation ω (please refer to the *Direct and Inverse Kinematics* section).

For horizontal displacements, it is necessary to add some sensors on the tires from the other side of the car. Other tasks could be assigned to this system (i.e., analyzing the information from all the four tires, scanning the planarity of the car, vibrations, installation of new sensors providing different types of information, etc).

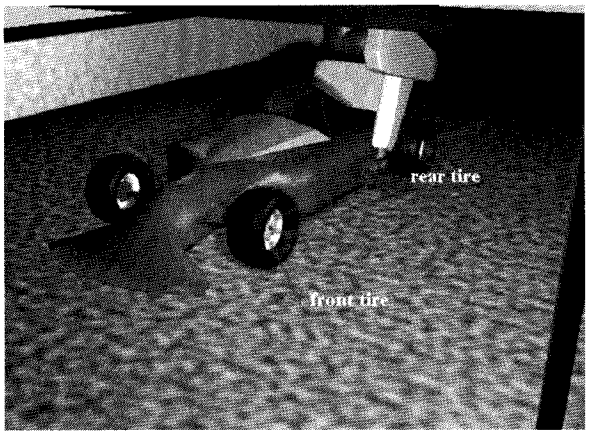

Figure 39. Sensor locations.

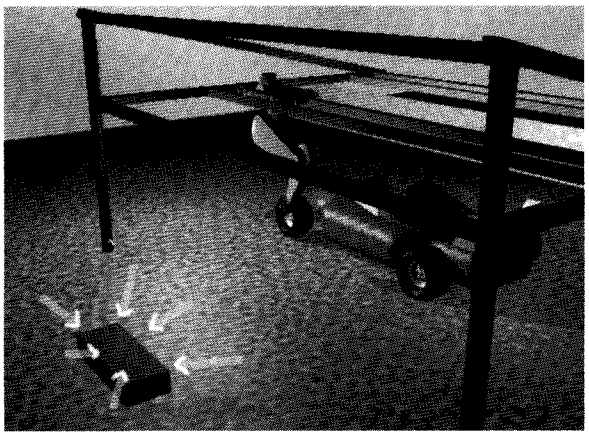

Figure 40. Scanning point.

6. Controlling and Supervising

The system will work perfectly independent for at least a couple of hours, more exactly it will be able to handle up to 5 tire changing sessions per car during a race, without any technical assistance needed. In order to assure this quality, supervising and controlling will be done from a control room located in the proximity of the pits.

6.1. TASKS IMPLIED

We need to be able to analyze at any moment the following parameters:

- for each engine manipulator, response per input power, activation requests and discrepancy between request and reply, internal functionality status,

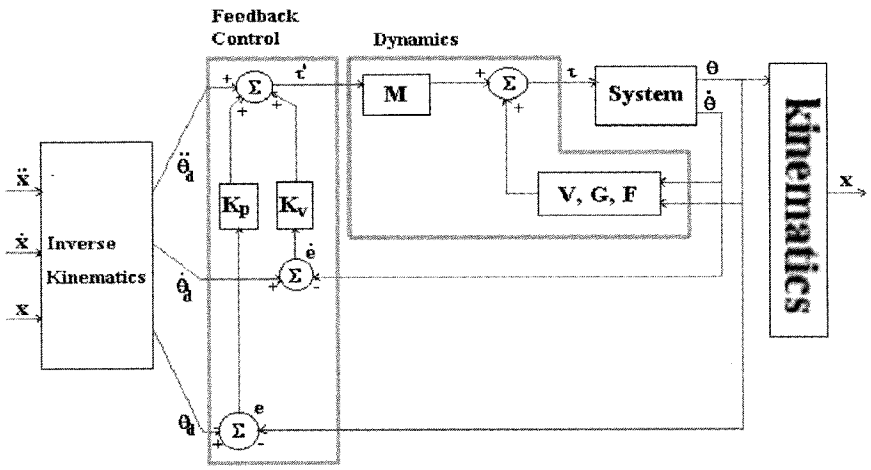

Figure 41.

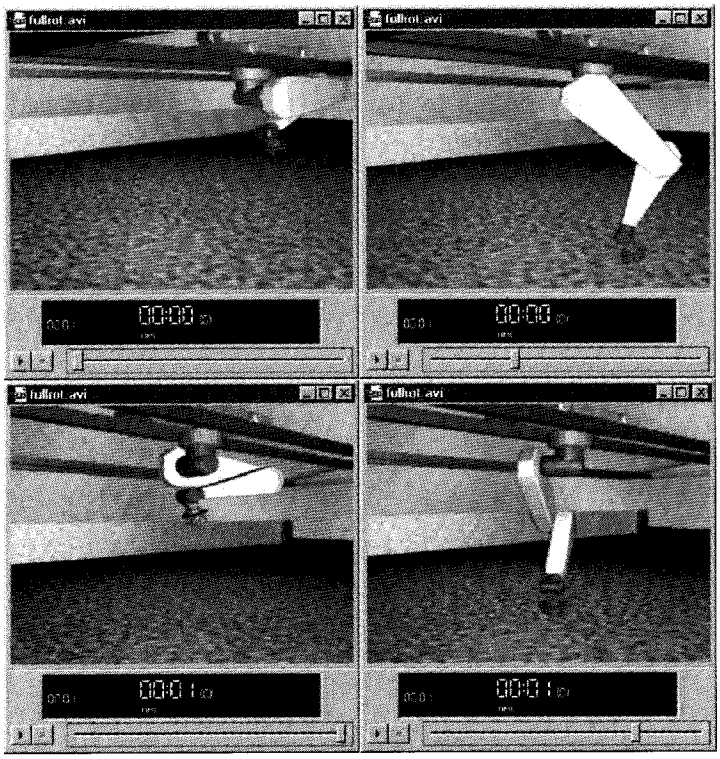

Figure 42. Simulation sequence.

- joint position and orientation, difference between requested revolution angle and the resulting one, smoothness of revolution, response time delay,
- link position and orientation, difference between requested and resulting position, synchronization with the joints,
- mass distribution in each arm, vibration factor evolution,
- sensor system supervising:

  – evolution of the delay in answering,
  – discrepancy between the detected position of the holes and the real one deducted from the final correction of the end-effector,
  – internal functionality status,

- tire sensors displacement in time, sensor functionality and reply frequency,
- support displacement and internal tension during arms motions, vibration and material response,
- temperature and pressure of the environment, wind velocity and direction as well as temperature evolution for each of the engine,
- parameter analysis evolution and general system status.

The required joints positions and orientations will be always pre-simulated and compared with the ones obtained from the direct sensor output. The parameter differences will be corrected using mostly PID control.

We implement digital feedback controllers for the system using a proportional plus derivative (PD) control [10, 17, 19], simplifying considerably the nonlinear dynamic equations, but also requiring a high update rate. We use a dynamic model for the simulation and control (Figure 41). To avoid jamming due to collision with other objects or parts, impedance control algorithms are to be considered too.

6.2. FLEXIBLE PARAMETER ANALYSIS

The data received from the sensing board of each arm has to be interpreted and displayed. Most of the parameters have to be shown graphically and forecasting functions have to be used. Good proximity forecasting functions [15, 16] will help a lot in the identification of recoverable damages.

Normally one of the controlling stations will display a real time recording of the coordinated arm, a simulation view showing the requested motion, actual position and simulated response of the arm.

6.3. CURRENT DEVELOPMENT STAGE AND RESULTS

Currently the robot CAD module is functional and is connected with the kinematics and dynamics modules. Animation and simulations showing the entire tire changing process has been done too. The following example (Figure 42) shows

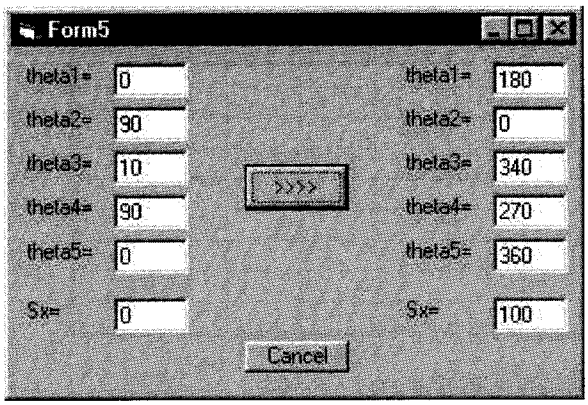

Figure 43. DK parameters.

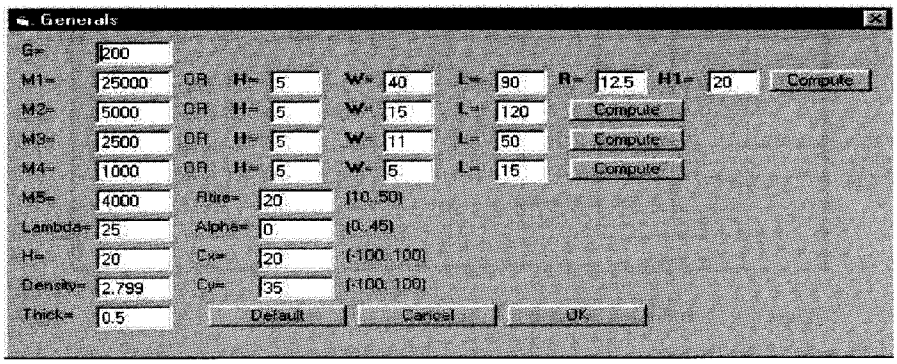

Figure 44. General parameters.

graphically the torque that has to be applied on 3 joints for a full tire changing process.

The DK parameters which have been used are shown in Figure 43. Some of the general geometrical and physical parameters that have been used are shown in Figure 44.

The torque distributions for 3 joints, considering these inputs and a 1-second relocation move is shown in Figures 45–47. The maximum and minimum values of the torque applied are shown, the time interval varies from 0 to 1.

7. Conclusions and Future Work

The main advantage introduced by the semi-autonomous system proposed here is the elimination of the human risks (no more team members required in the vicinity of a car). The five manipulators are able not only to change the tires of a car and refuel without assistance, but to obtain critical parameters of the car and interpret them in real-time.

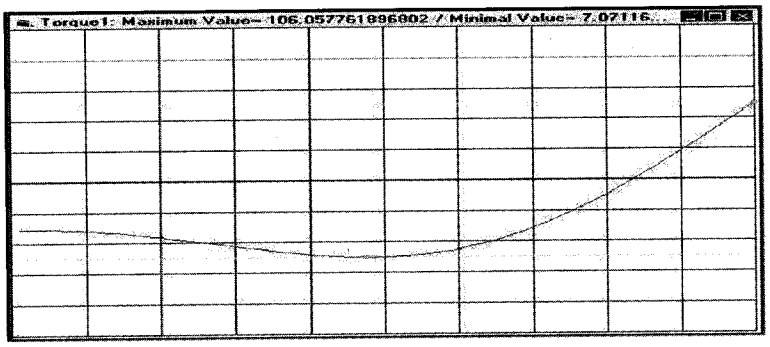

Figure 45. Torque 1 distribution in the interval of a second.

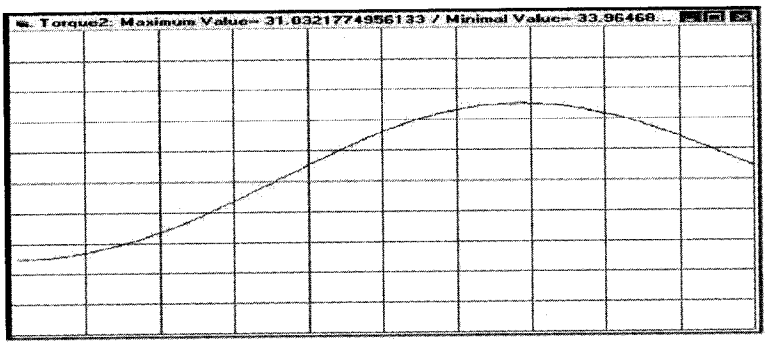

Figure 46. Torque 2 distribution in the interval of a second.

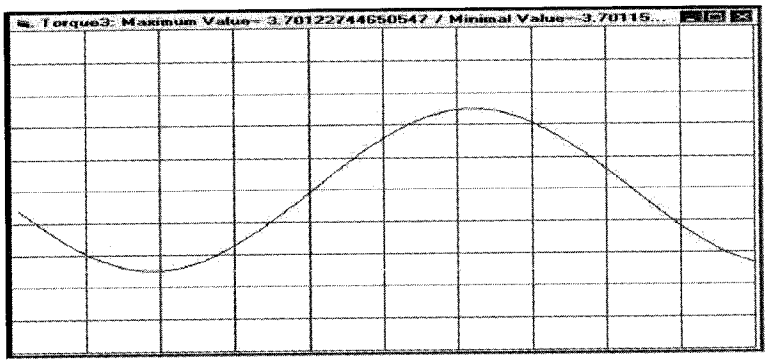

Figure 47. Torque 3 distribution in the interval of a second.

The second advantage is the low-variance time for pit stops for any team. Once a prototype will be ready, further optimizations will allow minimization of this time (currently estimated at 10 s).

Future work will address the refueling manipulator and complete the integration of the entire system within the FIA restrictions.

References

1. Spong, W. M.: *Robot Dynamics and Control*, Wiley, New York, 1989.
2. McKerrow, P. J.: *Introduction to Robotics*, Addison Wesley, Reading, MA, 1991.
3. Dekhil, M., Sobh, T. M., Henderson, T. C., Sabbavarapu, A., and Mecklenburg, R.: *Robot Manipulator Prototyping (Complete Design Review)*, University of Utah, 1994.
4. Nakamura, Y.: *Advanced Robotics – Redundancy and Optimization*, Addison-Wesley, Reading, MA, 1991.
5. Marris, A. W. and Stoneking, C. E.: *Advanced Dynamics*, McGraw-Hill, New York, 1967.
6. Christie, D. E.: *Intermediate College Mechanics*, McGraw-Hill, New York, 1952.
7. De Wit, C. C., Siciliano, B., and Bastin, G.: *Theory of Robot Control*, Springer, London, 1996.
8. Sobh, T., Dekhil, M., Henderson, T. C., and Sabbavarapu, A.: Prototyping a three-link robot manipulator, in: *The 2nd World Automation Congress, 6th Internat. Symp. on Robotics and Manufacturing* (ISRAM '96), Montpellier, France, May 1996.
9. Herrea-Beneru, L., Mu, E., and Cain, J. T.: Symbolic computation of robot manipulator kinematics, Department of Electrical Engineering, University of Pittsburgh.
10. Rieseler, H. and Wahl, F. M.: Fast symbolic computation of the inverse kinematics of robots, Institute for Robotics and Computer Control, Technical University of Braunschweig.
11. Dekhil, M., Sobh, T. M., Henderson, T. C., and Mecklenburg, R.: UPE: Utah prototyping environment for robot manipulators, in: *Proc. of the IEEE Internat. Conf. on Robotics and Automation*, Nagoya, Japan, May 1995.
12. Schalkoff, R. J.: *Digital Image Processing and Computer Vision*, Wiley, New York, 1989.
13. Hervé, J., Cucka, P., and Sharma, R.: Qualitative visual control of a robot manipulator, in: *Proc. of the DARPA Image Understanding Workshop*, September 1990.
14. Banks, M. J. and Cohen, E.: Realtime B-spline curves from interactively sketched data, in: *Proc. of the 1990 Sympos. on Interactive 3-D Graphics*, ACM, March 1990.
15. Thingvold, J. A. and Cohen, E.: Physical modeling with B-spline surfaces for interactive design and animation, in: *Proc. of the 1990 Sympos. on Interactive 3-D Graphics*, ACM, March 1990.
16. Li, Y. and Wonham, W. M.: Controllability and observability in the state-feedback control of discrete-event systems, in: *Proc. of Conf. on Decision and Control*, 1988.
17. Benedetti, R. and Risler, J. J.: in: *Real Algebraic and Semi-algebraic Sets*, Hermann, Paris, 1990, pp. 8–19.
18. Allen, P. K.: *Robotic Object Recognition Using Vision and Touch*, Kluwer Academic Publishers, Norwell, MA, 1987.
19. Craig, J. J.: *Introduction to Robotics. Mechanics and Control*, 2nd ed., 1989, Addison Wesley, Reading, MA, 1989.